

Waveform design for electroseismic exploration

Scott C. Hornbostel¹ and A. H. Thompson²

ABSTRACT

In earlier work, we described field tests that successfully detected electromagnetic-to-seismic (ES) conversions from gas sands and carbonate reservoirs. ES conversion amplitudes measure the electric properties of permeable rock with near-seismic resolution. This information is a new indicator of hydrocarbons. ES conversions produce small seismic responses. Detecting these signals requires high-power electromagnetic sources and high-sensitivity detectors. Extraction of signal from noise also requires sophisticated signal processing. Here, we describe coded waveforms of binary sequences optimized for the expected signals. These coded waveforms distinguish between linear and nonlinear conversions. We detected both linear and nonlinear conversions in field studies. Novel, high-power signal generators synthesize the required sequences from three-phase power lines. The electroseismic exploration system includes optimized source electrodes and digital accelerometers that are free of electromagnetic interference.

INTRODUCTION

Thompson et al. (2005) reported on case studies demonstrating that electromagnetic-to-seismic (ES) conversions can be used to image gas and oil accumulations. These studies detected gas sands to a depth of 1000 m and oil accumulations in carbonates to 1500 m.

In the ES method, voltage applied to grounded dipole electrodes drives current into the ground (Figure 1). The distance between the grounded electrodes and the length of the electrodes are comparable to or greater than the depth of the target. The massive electrodes have low electric resistance so that a low voltage will create large currents. Power waveform synthesizers (PWS) supply electric power to the electrodes at low voltage, ~ 120 V, and high current, ~ 1000 A.

ES conversions occur at rock boundaries where there is a gradient in electric properties. The source electrodes need to be of low resis-

tance and the source needs to supply power at the highest current possible because the ES conversion amplitude is related to the applied current.

There are several mechanisms for ES conversion. In one of the mechanisms, electrokinetic conversion, the applied current displaces ions in pore fluids lying near the pore surface. The polarization of the pore-surface electric fields creates relative motion between the pore fluid and the pore wall. The resulting inertial drag induces a pressure gradient in the grain space. This pressure gradient, integrated over all grains, is a macroscopic pressure that produces a seismic response (Pride, 1994). The seismic response is an exploding reflector, a concept discussed in detail in seismic literature (e.g., Claerbout, 1985).

In addition to electrokinetic coupling, there are other ES conversion mechanisms. These additional conversion processes may yield either first-order conversions, where the seismic response has the same frequency as the electromagnetic source, or higher-order conversions (Hornbostel et al., 2003), where the seismic frequency is a multiple of the electromagnetic source frequency. Two mechanisms illustrate higher order conversions. The first is electrostriction (Corson and Lorrain, 1962). An applied electric field generates an internal field at a rock boundary. In turn, the applied field interacts with the induced field, increases surface stresses and compresses the rock. This coupling is fundamentally second order, yielding a doubling of the frequency and an amplitude proportional to the square of the applied electric field.

Coupling to the spontaneous potential has been suggested as a second possible nonlinear coupling mechanism (A. H. Thompson, personal communication, 2006). Electrochemical potential gradients at rock boundaries generate the spontaneous potential. The resulting macroscopic internal electric field may couple to the applied field. An applied field that is comparable to the internal field alters the internal field significantly. This coupling of fields is analogous to rectification of current at a semiconductor p-n junction (Ashcroft and Mermin, 1976). The expected electromagnetic and ES responses occur at harmonic frequencies with amplitudes that are proportional to the first power of the applied field. Coupling to the spontaneous potential may also create high-order events in electromagnet-

Manuscript received by the Editor May 10, 2006; revised manuscript received November 9, 2006; published online March 1, 2007.

¹Exxon Mobil Upstream Research Company, Houston, Texas. E-mail: scott.c.hornbostel@exxonmobil.com.

²Houston, Texas. E-mail: athompson4@houston.rr.com.

© 2007 Society of Exploration Geophysicists. All rights reserved.

ic surveying, such as the spectral induced polarization (IP). It may be possible to use the same ES binary sequences to improve the signal-to-noise ratio (S/N) in IP surveys to detect reservoir boundaries.

The full ES conversion problem is separated into three independent parts: propagation of the electromagnetic stimulus to the target, conversion to the seismic wave, and propagation of the seismic wave to the surface (White, 2005). We are concerned only with the vertically propagating P-wave. In this case, only the vertical component of the electric field at the target is relevant.

Attenuation of the electromagnetic stimulus with depth, and the small ES conversion efficiency, yield a small ES seismic response. To enhance these small signals, we designed a method that maximizes the electric power by using generators capable of megawatt output. We optimized the detection system with a 2D array of digital accelerometers. Digital accelerometers, based on MEMS technology, are immune to electromagnetic interference from the source electrodes. Even with a high-power source and an array of sensitive detectors, the signal is expected to be several orders of magnitude below the random background noise. Enhancement of the signal-to-random-noise ratio requires many repetitions of the source. For maximum time efficiency, the signal waveform fills most of the clock time. Correlation of the signal and source waveforms discriminates against random noise. We require a source waveform that will not introduce artifacts in the time window where signal is expected. In this paper, we describe waveforms from the general class of binary sequences that satisfy these requirements.

From the initiation of field research in 1987, we expected to see both first-order and higher order ES conversions. In the first east Texas test we describe, we successfully detected first-order conversions at a gas sand interval. We also detected second-order conversions but our processing was not yet robust enough to be confident of the results. In the second, much larger test in west Texas, we were not able to detect the first-order conversions because of noise coherent with the source, but we improved the processing and were able to detect the higher order response. Detection of the higher order response was possible because the processing effectively rejected first-order noise from the source.

We begin this paper with a description of the binary sequences used for linear and nonlinear processing. We next discuss waveform

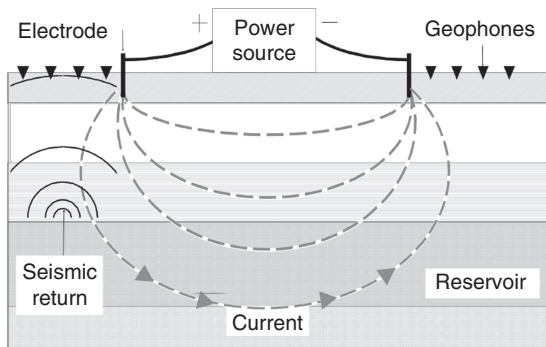


Figure 1. Schematic diagram of a typical field implementation of ES surveying. A power source drives current through electrodes in contact with the earth. The current penetrates the subsurface to a target where the electric field interacts with existing electric fields at rock boundaries. This interaction causes stresses that propagate away from an interface as seismic waves. The electrodes are typically buried wires. Geophone arrays, placed outside the electrode pairs, detect the returning seismic waves.

generation and the field implementation of the coded sequences. In the processing section we discuss two case studies, one of first order and one of higher order. Further descriptions have been, or will be, published elsewhere on field methods, geological models of ES conversion, and mechanisms for higher order conversions (A. H. Thompson, personal communication, 2006), numerical model construction in a layered earth (B. S. White, personal communication, 2006), mathematical solutions of the complete ES conversion problem in three dimensions (White, 2005), and the history of ES studies and a summary of recent advances in ES methods (A. H. Thompson, personal communication, 2006).

WAVEFORM DESIGN

Field tests and ES modeling (Thompson et al., 2005) have shown that the amplitude of ES signals at the surface varies from about 10^{-9} m/s down to about 10^{-13} m/s, or smaller. The range of depths in these evaluations was from 100 m to 2 km and the source current ranged from several hundred to over a thousand amperes. Typical signals ranged from two to six orders of magnitude below the expected ambient random noise level of $\sim 10^{-7}$ m/s. As a result, many repetitions of long source sequences were required to obtain sufficient S/N. Some comments are included in Appendix A on the dynamic-range implications for detection of small signals.

The electromagnetic source signal travels to the target at an effective speed that is ~ 100 times faster than a seismic wave. In comparison to characteristic seismic traveltimes, the target is effectively excited simultaneously across its full extent. The seismic wave produced at the target propagates back to the surface at seismic velocities. If the amplitude is large, the moveout of the signal can be measured from the edge of a structure. Here, we concern ourselves only with the vertically traveling P-wave. The one-way seismic traveltime determines the depth to the target. The coded source sequence must have sufficient bandwidth to resolve the arrival times from horizons of interest. In addition, the correlation side lobes of the source waveform must be low enough and displaced in time far enough so that strong-signal side lobes do not obscure later, weaker signals. To address these needs, we created waveforms from three-phase, 120 VAC, 60 Hz power lines by rapidly switching among the three phases and between the two polarities of each phase. The selected waveforms are in the family of binary-coded waveforms.

A binary-coded waveform consists of a sequence of elements of varying polarity. In our work, we call attention to the advantages of using elements based on the power-line sine wave. The individual element might be, for example, a single cycle at 60 Hz. In a coded waveform, the choice of waveform elements optimizes the frequency content of the source to achieve high depth resolution. The length and structure of the binary sequences minimize correlation side lobes.

The correlation of the binary-coded waveform, with its reference, will give a main wavelet that is the autocorrelation of the individual waveform element. As an example, consider the single cycle at 60 Hz in Figure 2a. Its autocorrelation and the related frequency spectrum are to the right of the element. This range of frequencies is adequate for imaging shallow targets. Three-phase power permits construction of both higher and lower frequencies. Figure 2b is an example with a nominal frequency of 22.5 Hz. The broader wavelet and lower frequencies shown in Figure 2b allow penetration to deeper targets.

The correlation of the binary-coded waveform with its reference produces side lobes in addition to the main wavelet. Such side lobes occur earlier or later in time and can appear to be ES signals. For example, if there is a strong ES conversion near the surface, then correlation side lobes may appear at later times, suggesting an ES conversion at greater depth. It is essential to minimize the amplitude of the side lobes and to push them to later times where they will not be confused with weak signal. Two types of binary sequences are well suited for ES waveforms. One is the Golay complementary sequence pair (Golay, 1961) and the other is the maximal length shift-register, or pseudorandom binary sequence (Golomb, 1964). Configurations of these sequences can minimize correlation side lobes and optimize the time position of the highest amplitude side lobes. The conversion mechanism and the frequency stability of the power supply also constrain the type of binary sequence and its length. When frequency drift is substantial, a shorter sequence is required. Field tests and computer modeling guide selection of the acceptable waveforms for an acquisition program.

Linear (Golay) sequences

Golay complementary sequence pairs (Golay, 1961; Hornbostel and Thompson, 2002) are useful for linear ES detection. A binary Golay complementary pair of sequences comprises two sequences that are of the same length and for which the autocorrelation of one sequence has the opposite polarity to that of the autocorrelation of the other, except at zero lag. The essential property of such complementary pairs is that the sum of the autocorrelation functions is zero everywhere except at the center wavelet. An illustrative pair of length eight using the binary sequences $(-1 -1 -1 1 -1 -1 1 -1)$ and $(-1 -1 1 1 1 1 -1 1)$ with a 60-Hz element is shown in Figure 3.

Figure 4 shows the autocorrelations and the sum of the autocorrelations for this example. Theoretically, the resulting sum has no side lobes. The sequence-pair approach is efficient in the sense that the waveform is continuous; that is, without breaks. Proper side lobe cancellation, however, depends on subtraction of the large side lobes in Figure 4a and b. The subtraction would be imperfect if, for example, there was frequency drift in the power supply or fluctuation in the signal amplitude. Scaling the data to match amplitudes and selecting Golay pairs with small side lobes prior to summation minimizes these problems.

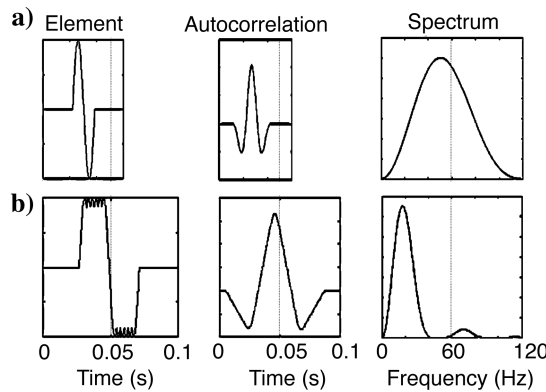


Figure 2. (a) 60-Hz waveform element and its autocorrelation and frequency spectrum; (b) 22.5-Hz waveform element, created by synthesis from a 60 Hz three-phase power source, and its autocorrelation and frequency spectrum.

For a field implementation, one might choose a 60-Hz waveform element and a Golay sequence of length 1664 (27.7 s). Kounias et al. (1991) discussed methods for constructing Golay sequences of different lengths. Possible sequence lengths are of the form: $2^{j}10^k2^{l}$ where j , k , and l are integers. For a given sequence length, there are many possible sequence pairs. An exhaustive numerical search to select pairs with minimal side lobes is one way to find an optimal pair for a given length. Ideally, the sum of two such Golay sequence autocorrelations cancels all the side lobes. In practice, frequency drift and amplitude fluctuations between records limit the cancellation. It is advisable to minimize the side-lobe energy of the individual autocorrelations prior to summation. The sequences used in the field were obtained through a numerical search to find small side lobes for each autocorrelation, combined with the practical criterion that the sequence was as long as possible, subject to limits imposed by power line stability and data collection parameters.

Nonlinear (PRBS) sequences

When the expected ES signal occurs at even multiples of the source frequencies, a combination of pseudorandom binary se-

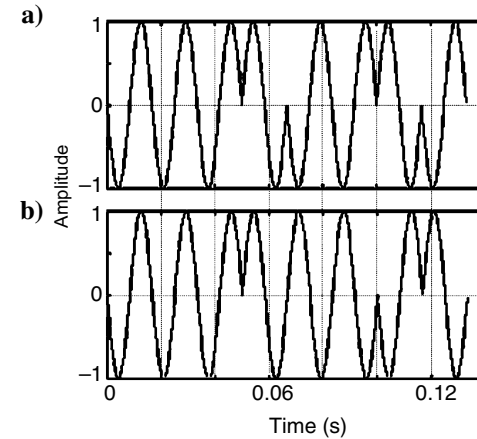


Figure 3. (a) and (b) A pair of eight-element Golay complementary sequences with a 60-Hz element.

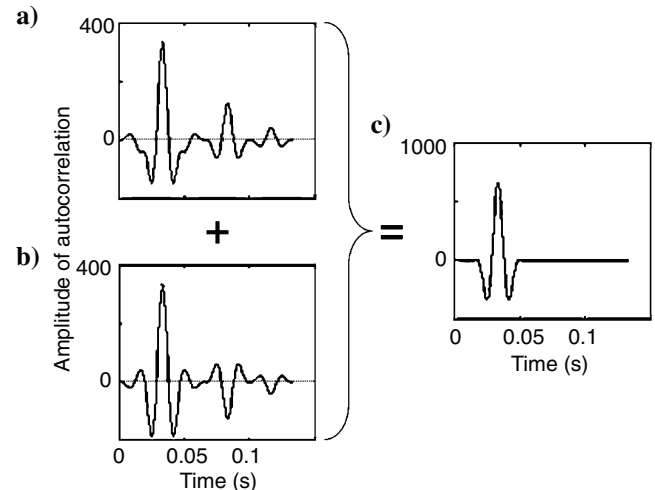


Figure 4. (a) and (b) Autocorrelations of the Golay waveforms of Figure 3; (c) the sum of these autocorrelations.

quences (PRBS) is most useful. Consider the case in which the seismic response is proportional to the square of the input current. This case leads to a doubling of the input frequencies. The squaring assumption is optimal for some nonlinear mechanisms, such as second-order electrostriction, and still allows detection of other mechanisms that have some second-order components in the signal. When one is looking for nonlinear conversions, the linear signals are a noise source. Linear noise can come from electromagnetic pickup in the receiver system as well as from induced seismic noise at the source electrodes, excitation of field infrastructure, or the linear ES effect in the subsurface. The waveform design must discriminate effectively against noises linearly related to the source waveform. A modified version of the maximal length shift-register sequence (Golomb, 1964) can be adapted to address these issues.

Modifying PRBS sequences to retain second-order conversions

The PRBS, also known as the shift-register sequence, is a binary $\{1, -1\}$ sequence of length $2^n - 1$. (Note that we use the braces “{}” to represent an alphabet of elements to be drawn on for a given sequence type.) Figure 5a is an example of length 7 with a 60-Hz element (i.e., $-1 \ 1 \ -1 \ 1 \ 1 \ 1 \ -1$). Figure 5b is the circular autocorrelation of Figure 5a. A circular autocorrelation is used because a PRBS sequence is designed to be repeated multiple times, end to end, in a single data set. The central waveform is the autocorrelation of a 60-Hz cycle and the side lobes are 60 Hz with relative amplitude of 1/7. The amplitudes of the side lobes are inversely proportional to the sequence length. The PRBS sequence, as it stands, is not useful for nonlinear ES detection because the squaring mechanism removes information coded in the $\{1, -1\}$ polarity reversals.

A modification suggested by Foster and Sloan (1972) to address the side lobe problem is useful for the nonlinear detection problem. In this case, the waveform is altered to include only the positive binary elements (Figure 6a). In other words, a signal of zero amplitude replaces the polarity-reversed elements and the $\{1, -1\}$ alphabet is replaced with a $\{1, 0\}$ alphabet. When circularly correlated with the original sequence (Figure 5a) the result now has zero side lobes (Figure 6b).

After squaring, the ES return is as shown in Figure 7a and is still a $\{1, 0\}$ sequence, but with the basic sequence element now a squared

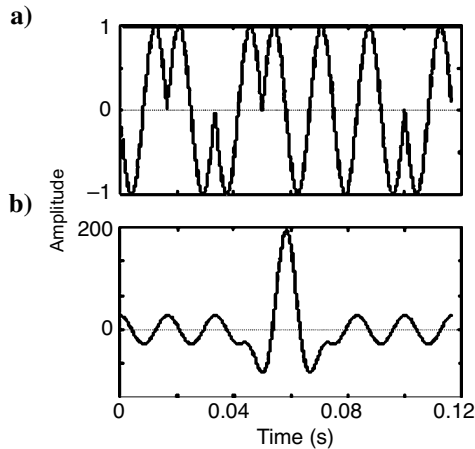


Figure 5. (a) Maximal length shift-register sequence with a 60-Hz element; (b) its circular autocorrelation.

cycle of 60 Hz. As in the case above, a $\{1, -1\}$ generated reference is needed to correlate with this expected signal. The squared $\{1, -1\}$ reference is illustrated in Figure 7b and the circular correlation of Figure 7b with Figure 7a gives the result shown in Figure 8a after removal of low frequencies.

Removing first-order noise during second-order detection

One drawback to this approach is that a linear return, proportional to Figure 6a, will produce an artificial nonlinear signal when correlated with reference Figure 7b. Figure 8b shows this cross-term. Another two-stage use of the PRBS minimizes this effect. In the first stage, the $\{1, 0\}$ input signal (Figure 6a) is modified to a $\{1, -1, 0\}$ input as in Figure 9a. The squared response (Figures 7a, 7b, and 8a) is unchanged because the nonlinear mechanism converts the $\{1, -1, 0\}$ sequence into a $\{1, 0\}$ sequence, squaring the sequence removes all the negative elements. The difference is that this correlation shifts

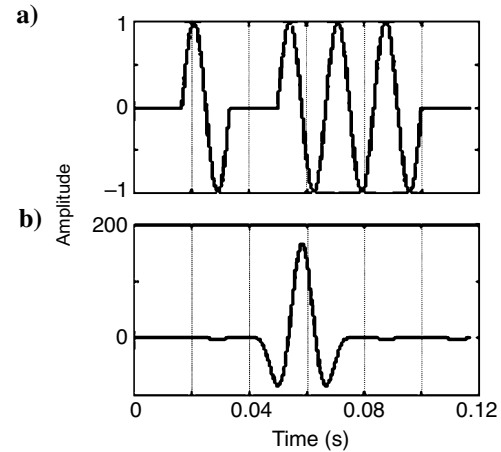


Figure 6. (a) A shift-register sequence with zeroed-out elements; (b) the circular crosscorrelation of this sequence with the original shift-register sequence of Figure 5a. The circular crosscorrelation has zero side lobes.

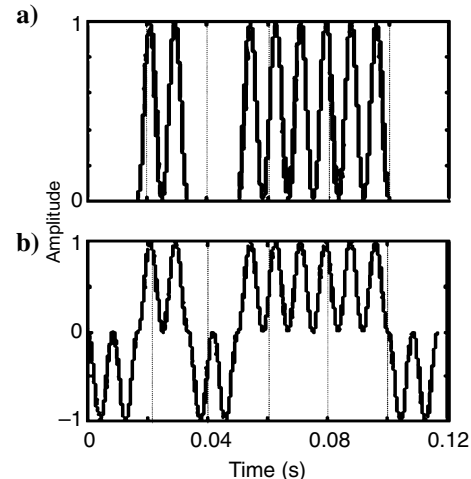


Figure 7. (a) The squared response from the input sequence of Figure 6a; (b) the associated reference with negative squared elements included.

the nonlinear artifact induced by the linear noise to a later time. Figure 9b illustrates the unwanted nonlinear noise induced when a linear return (Figure 9a) is correlated with a nonlinear reference (Figure 7b). This crosscorrelation noise occurs at later time, compared with that in Figure 8b.

The selection of the cycles to reverse is important. The preferred approach is to multiply the input sequence, Figure 6a in this case, with a circularly rotated version of the $\{1, -1\}$ reference binary sequence; that is, the sequence that generated Figure 5a. This binary sequence is uncorrelated with the input sequence except at the rotated lag. The reason for this lack of correlation comes from the pseudorandom sequence theory. This is the same reason that Figure 5a correlated with Figure 6a produces no side lobes. This rotated $\{1, -1\}$ scaling sequence delays the unwanted correlations.

The second stage in reducing linear–nonlinear correlation effects is to repeat the experiment using a polarity-reversed input sweep as in Figure 10a (cf. Figure 9a). The squared response (Figures 7a, 7b, and 8a) is again unchanged, but the linear–nonlinear correlation

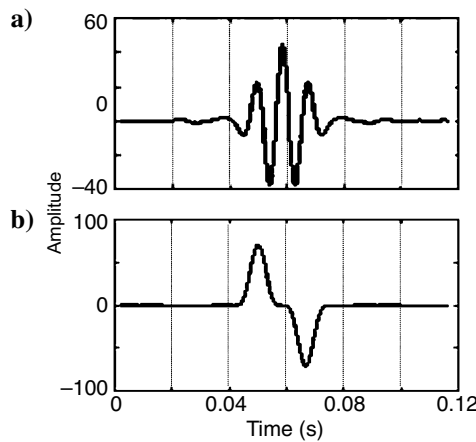


Figure 8. (a) The nonlinear signal resulting from circular cross-correlation of the squared response of Figure 7a and associated nonlinear reference of Figure 7b after removing the low frequencies; (b) the unwanted cross-term from correlating the linear signal of Figure 6a with the nonlinear reference of Figure 7b.

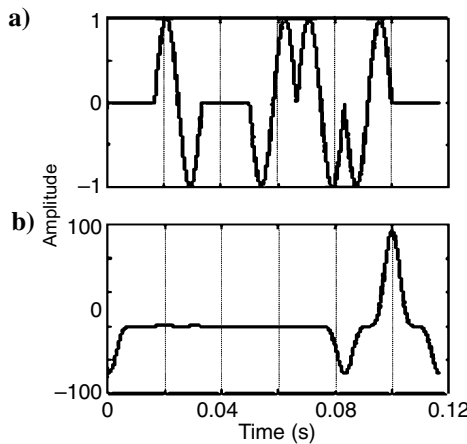


Figure 9. (a) The modified shift-register sequence with zeroed-out zones and polarity reversals; (b) the unwanted cross-term from correlating the linear signal of Figure 9a with the nonlinear reference of Figure 7b.

(Figure 10b) has its polarity reversed (cf. Figure 9b). Adding the results of the two correlations doubles the desired signal (Figure 8a) while removing the unwanted linear effect.

Theoretically, this polarity reversal in the second stage works without the $\{1, -1, 0\}$ scaling, but it is better to include the delay, because the remaining residual effects caused by experimental inaccuracies will occur later in the data and will not interfere with the desired signals.

Figure 11 is a composite of Figures 6–10 that summarizes the features of the second-order processing. The upper line of graphs shows how the processing passes a signal that is the square of the source waveform. Figure 11a and b illustrate suppression of the linear-signal artifact by simple polarity reversal. (The correlated results will be summed to remove the artifact.) Figure 11c and d illustrate removal of the linear-signal artifact by delay of the artifact with $\{1, -1\}$ scaling in addition to simple polarity reversal.

The short element sequences shown in the figures here are just for illustration. In a typical field experiment, one might use several repeated 255-element sequences (4.25 s each at 60 Hz) to create a single record. Note that repetition of the sequence is required for PRBS sequences with circular correlation. In this case, the unwanted linear–nonlinear correlation can be pushed halfway (i.e., to about 2 s) to remove it from the times of interest. The $\{1, -1, 0\}$ input sequence can then be squared and modified with negative squared elements (as in Figure 7b) to give a reference for circular correlation. This concatenated record would typically be run hundreds of times for signal-to-noise enhancement.

These PRBS waveforms are also suitable to address the more general problem of detecting nonlinear conversions in other applications, such as harmonic distortion in seismic vibrators, or nonlinearity in spectral induced polarization.

FIELD IMPLEMENTATION

Waveform generation

Generating coded, electromagnetic waveforms at the scale required for hydrocarbon exploration requires new equipment. The waveform generators must:

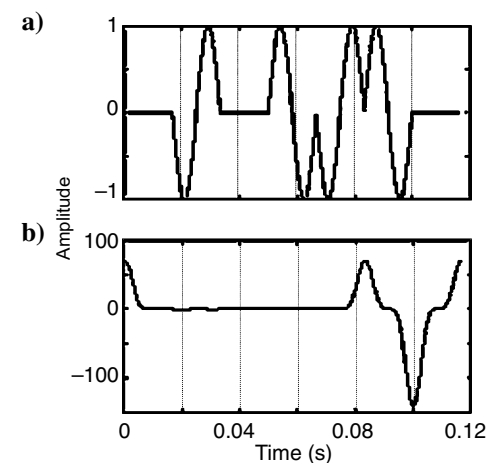


Figure 10. (a) The shift-register sequence with zeroed-out zones and opposite polarity reversals; (b) the unwanted cross-term from correlating the linear signal of Figure 10a with the nonlinear reference of Figure 7b.

- produce megawatt power levels at voltages of several hundred volts and a few thousand amperes
- minimize waste heat and total power consumption
- create waveforms specifically designed for the intended target
- be transportable for field use
- utilize line and generator power
- run continuously in harsh environments
- require minimal attention over days of data collection
- satisfy stringent health, safety, and environmental standards

A system called the power waveform synthesizer (PWS) meets these requirements. Each PWS contains the circuitry shown in Figure 12 and acts as an independent unit. The power output of a single PWS is 350 kW at 120 V. Combinations of single units, in series or parallel, provide additional flexibility. Input power is supplied by three-phase power lines or by one or more generators. Generators are preferred because they often are more stable over time. This stability reduces correlation side lobes in data processing and permits real-time data stacking.

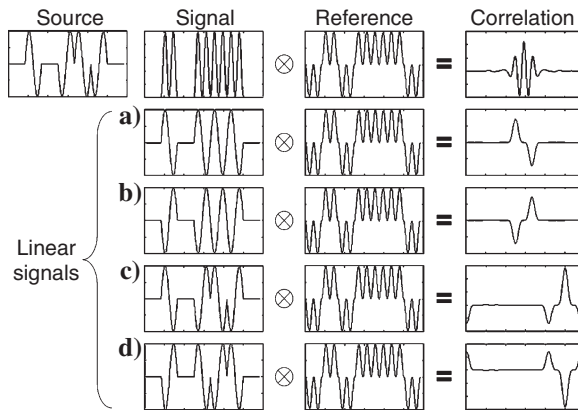


Figure 11. Illustration of the features of second-order processing. The top row shows the linear source waveform that ES conversion squares to yield the signal. The signal is correlated with the reference to produce the central wavelet of the squared response. (a) and (b) are a pair of PRBSs of opposite sign used to reject the linear signal that leaks through the squared processing. The correlations in (a) and (b) are artifacts that have opposite signs so that summing them removes them from the processed signal. (c) and (d) are two ternary sequences used to reject and delay the artifact produced when the linear signal is processed with the squared processing.

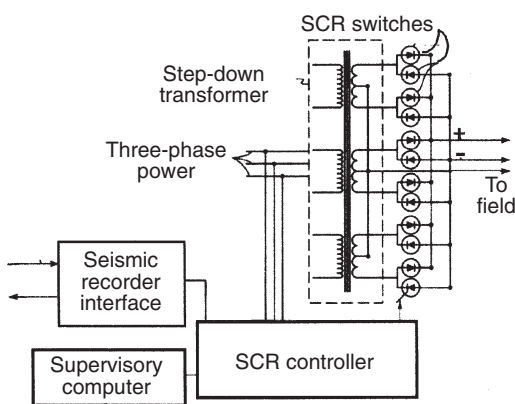


Figure 12. Block diagram of a PWS.

The PWS power requirements are determined by modeling the average electric field at depth and then estimating the amplitude of the ES response from the target. The minimum detectable ES amplitude then improves in proportion to the square root of the number of repetitions in the stack. We constrained the stacking with a practical limit of ~ 1000 repetitions. This calculation may underestimate the ES response and overestimate the required power because the calculation does not accurately model the electric inhomogeneity of the subsurface. Increased inhomogeneity often increases the ES response (Thompson et al., 2005). For targets 1000 m deep, or greater, in locations where the overburden resistivity is only a few ohmmeters, these calculations indicate a need for megawatt power levels. In practice, the maximum power that is feasible to transport to the field also limits the source configuration. Six hundred kilowatts of power produced images of the 1500-m-deep target at the west Texas test site. This result is encouraging for applications requiring greater depths.

In Figure 12, the input voltage on the primary side of a three-phase step-down transformer is 480 V. This voltage is typically available from generators or from standard power line transformers. Each of the three independent transformers is wired to one phase of the power line on the input. The secondary windings of the transformers feed a set of twelve silicon-controlled rectifier (SCR) switches that select portions of each of the three-phase voltages to construct a desired waveform. The outputs from the PWS go directly to the electrodes in the field.

Figure 13 shows how to use a three-phase input to construct waveform elements of variable frequency at, or below, the frequency of the power source (60 Hz). Each colored sine wave represents one phase of the power source. The dashed and dotted lines of each color represent the two possible polarities. The solid curve illustrates a selection of phases that produces 30 Hz waveform elements from this 60 Hz power supply. At each vertex, where one color joins another, the SCR can switch off one phase and turn on another.

The supervisory computer (Figure 12) contains the programmed binary sequence and instructs the SCR controller. The seismic recorder interface communicates the SCR switching information to the seismic data acquisition system to synchronize the systems. When multiple PWSs are operating, a central computer (not shown) triggers each PWS to start operation and establishes the time mark with the seismic system. A graphical user interface enables field personnel to operate the equipment.

Figure 14 shows the output sides of eight PWSs operating in a field installation. The output cables are insulated 4/0 copper that connect the PWSs to buried electrodes. The resistance of the cables is smaller than the resistance of the electrode–earth system. Figure 14 also shows several deployment details. A rigid frame under each PWS permits lifting the unit onto a truck with a forklift. Hard points

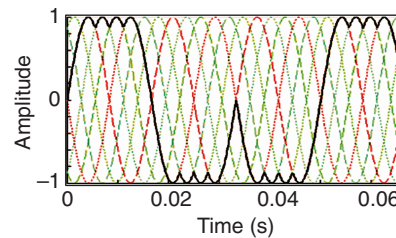


Figure 13. Construction of a low-frequency coded waveform by switching between phases of a three-phase power supply.

also enable lifting the units with a crane. Each PWS weighs approximately 2700 kg. The rigid supporting frame attaches to vibration-isolation supports. These supports minimize parasitic vibrations from the three-phase transformer that would otherwise transfer into the earth. Such vibrations would correlate with the transmitted coded signal and interfere with the data. In practice, we have not had to use the power from more than two PWSs at one time to generate measurable ES responses. Experience gained in our field tests suggests that future tests can be successful using substantially less equipment and wire.

Design and implementation of the PWS was a significant part of our ES research program. The fundamental problem is to control the switching of a thousand or more amperes of current in a time scale of tens to hundreds of microseconds, at the instant in time when two phases are at the same voltage. This switching is done while maintaining the fidelity of the waveform over the bandwidth of interest.

Field deployment

Figure 15 is an aerial view of the field layout we used for a series of ES experiments at a site in east Texas. The separation of the grounded electrodes is comparable to or greater than the depth of the target. This electrode separation generates a maximum vertical electric field at the target depth below the geophone locations south of the southern electrode.

The shape of the electrode that is distant from the geophones is not important; one or more well casings in a developed field may be used. The condition of a well used as an electrode is not important so long as the electric contact with the earth is good. The total resistance of an earth-electrode-wire system in a typical field test is 0.1 to 0.01 ohms. In Figure 15, an earlier experiment dictated the shape of the northern (distant) electrode. The shape of the distant electrode was assumed to have only a second-order effect on the shape of the electric field lines at the target. Modeling of the electric field at depth confirmed the validity of this assumption.

The electrodes near the geophone array typically form a linear arrangement of buried wire or a linear array of vertical pipes. In the east Texas experiments, we used three buried parallel wires. In other settings, the electrodes were vertical pipes about 3 m long. The advantages of vertical electrodes include rapid deployment and flexible positioning. The linear electrode near the geophone array does not need to be precisely linear. Deviations in linearity of 10% of the target depth will reduce to zero at the depth of the target because the wavelength of the EM wave is much greater than the deviations from linearity. This is of substantial benefit because it permits routing the electrode around existing infrastructure.

Conventional coiled-wire geophones can be problematic in that they immediately sense the large magnetic fields associated with the EM source. After correlation, this direct pickup appears as a huge signal at zero time. Correlation side lobes from this signal that appear later in time are commonly larger than the signals of interest, even when specially coded waveforms are used. Digital accelerometers based on MEMS technology are preferred because they are immune to direct EM pickup from the source.

A typical field protocol calls for several hundred coded sweeps, of about 60-s duration, for each geophone array and electrode setup. Collection of a data set for one electrode and geophone array may require one week of time. In future tests, improvements in equipment and implementation methods may reduce this time and permit roll-along data collection. A survey may use coded sweeps centered at a

single frequency or several coded sweeps centered at different frequencies to improve bandwidth. Several coded sweeps centered on different frequencies can improve bandwidth because they are collected separately and can be separately balanced. For example, we often encountered high inductance that was associated with the large current loop in the ground to the depth of the target. This inductance reduces the current at high frequencies from the constant voltage PWS. Increasing the number of repetitions of the high-frequency coded sweeps can improve the S/N and thus increase the usable bandwidth. Separate waveforms for both linear and nonlinear ES conversions may be included.

In addition to the ES data, several complementary data sets confirm the origin of the ES conversions and help with noise reduction. The suite of confirmation tests we used include:

- well data to verify that the ES conversions originate at a specific depth
- deep EM surveys (e.g., CSAMT) to help with modeling and confirm resistive anomalies
- near-surface resistivity to locate noise-producing infrastructure, such as buried pipes that couple to the electromagnetic source
- EM field measurements around the operating electrodes to investigate nonuniform current injection and detect possible noise sources from high or low conductivity regions



Figure 14. PWS in field operation, one is 2 m high, 2 m wide, and 3 m long.

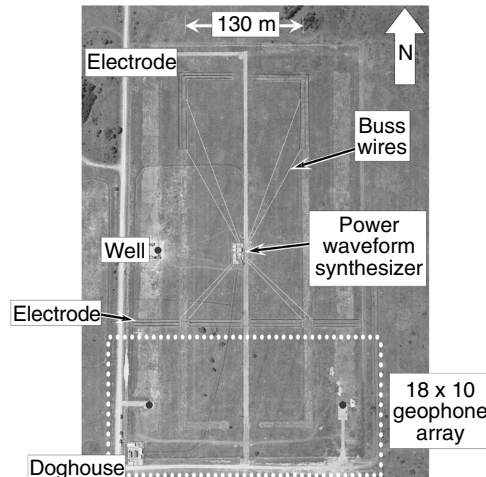


Figure 15. Field layout for east Texas experiments.

- horizontal-component seismic data to identify and suppress horizontally traveling noises
- seismic data collected from vibrators placed along the electrodes for later processing to mimic and remove unwanted seismic waves generated at the source

These various quality control and confirmation tests are part of our research program. They identify noise sources and confirm, or prove, that the detected ES signals originate from the target depth. Most of these tests will not be required in routine exploration applications.

PROCESSING

Processing of ES data begins with correlation and stacking of the many repetitions. The electromagnetic source energizes all points in the subsurface essentially simultaneously. For laterally extensive targets, the seismic energy propagates as a plane wave back to the surface. It is not necessary to perform NMO corrections, CDP sorting, or other velocity-related manipulations.

Much of the processing effort focuses on noise reduction. Editing of noisy traces removes 30% or more of the data collected. Noisy traces have anomalously high amplitudes or are traces that correlate with recorded surface noise at a particular accelerometer. Adaptive filters based on the least-mean-square algorithm (Widrow and Glover, 1975) remove noise that correlates with seismic data collected separately using vibrator sources located along the electrodes. The ES signal is primarily vertically traveling. Near-surface noise most likely generates horizontal motion, so we remove signal on the vertical accelerometers that correlates with the horizontal accelerometers.

Additional processing is similar to seismic data processing that includes dip filters for well data, band-pass filters, spatial mixing for noise reduction, muting of early noise arrivals, and pulse-shaping deconvolution. The following sections show examples of surface and well data from an east Texas test site and from a west Texas oil field in the Midland Basin. Thompson et al. (2005) give a more detailed discussion of these and other field tests.

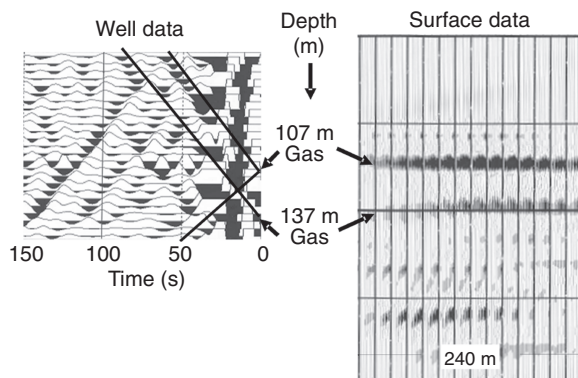


Figure 16. Linear ES well and surface data from the east Texas experiments. The cemented-in well geophone data illustrate possible ES conversions emanating from the gas sands at 107 and 137 m. The right panel shows the corresponding ES horizons in the surface data. The early (0–40 ms) noise in the well data is residual direct electromagnetic interference from the source. Data were processed with a pair of 60-Hz Golay sequences.

East Texas linear data

The processed ES data from the 18×10 geophone grid (250 \times 140 m) used at the east Texas test site (Figure 15) are shown in Figure 16. The display of surface data shows 140 stations of the total 180 stations in a 3D survey. Each small panel of data is a set of 10 time traces from south-to-north stations within the 18×10 grid. These time traces run perpendicular to the electrode. The 14 panels represent 14 of the west-to-east stations that are parallel to the electrode. This test used approximately 1000 repetitions of a 60-Hz Golay sequence of length 1664, a 27.7-s sequence with a 30-s total record length. Stacking experiments showed that ~ 100 repetitions produced an adequate S/N, so the data volume from 1000 repetitions was excessive. The strong signal between 70 and 100 ms is a combined ES response from two gas sands at 107 and 137 m depths. The first 50 ms of data have some residual electromagnetic-pickup noise remaining after summing matched coiled-geophone receivers. This residual noise has been muted out for the surface data in Figure 16. These problems with geophones led us to use digital accelerometers in later studies.

The residual pickup noise is evident in the well data in Figure 16. Even after cancellation from matched geophones, the residual pickup is a serious problem in the first 40 ms. The geophones cover the drilled depth interval from 6 (top trace) to 152 m (bottom trace) with 6-m spacing. We collected well and surface data concurrently.

The residual pickup noise obscures the most interesting interval for identifying the origin of the ES signal from the gas sand. Even so, the indicated up-coming and down-going paths show signals originating at the gas sands, as suggested by the extrapolation to zero time that is coincident with the depths of the gas sands.

West Texas nonlinear data

The west Texas site was chosen to test the application of ES conversions for oil reservoirs and carbonates. The targets are greater than 1500 m deep so this site also tested the technology to a much greater depth than at the east Texas site. This large increase of scale pushed our equipment to the limits of its capability. Even so, we were successful in detecting second-order conversions. (We had observed the second-order conversions at the east Texas site but with untested processing.) At the west Texas site, we found that the greater depth and weaker signal prevented extraction of the first-order signal from source noise. This led us to rework the second-order processing to reject source noise and thus detect the target signal.

The west Texas test required several changes to our methodology. We used PRBS sequences to image nonlinear conversions from stacked carbonate reservoirs from 1310 to 1615 m. Combined sets of PRBS sequences with element frequencies of 0, 8, 11, 15, 18, 22, and 25 Hz improved the bandwidth and S/N. These frequencies were selected because they were easily accessible from the 60-Hz source using our PWS hardware. There were about 600 repetitions at each of these frequencies with individual sequence lengths of 30 to 40 s. On the surface (right panel of Figure 17), digital accelerometers effectively eliminated direct EM pickup. Hydrophones in the test well were also insensitive to electromagnetic pickup. The surface data run along a 2D line parallel to the near electrodes and with about 100 m offset. The hydrophones cover an interval from 76 to 1216 m depth.

The basic processing used here is similar to that used for the east Texas test. One difference is the need to combine the multiple nonlinear sequences. The individual sequences are first band-pass fil-

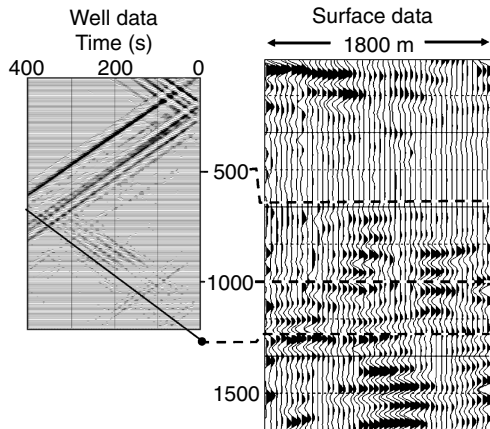


Figure 17. Nonlinear ES well and surface data from the west Texas experiments. Digital accelerometers on the surface and hydrophones in the well eliminated the electromagnetic interference. Shallow and deeper nonlinear ES conversions are evident. We used a set of PRBS sequences with frequencies up to 22.5 Hz.

tered to focus on the doubled frequencies generated by a squaring conversion. As an example, for a sweep centered at 8 Hz, the filter retained frequencies between 12 and 24 Hz. After filtering, we scaled the seven different frequency sequences prior to summation. Detailed pulse shaping could also be included in the processing sequence, but we did not use it in this test.

Figure 17 compares nonlinear well data with a line from the surface data. A signal in the well data appears as a sideways “V” that originates at a point in the subsurface at zero time. Three distinct shallow conversions are evident in the well, the first is likely from the surface. There are several strong signals from greater depth. This is surprising, given the reduced field strength expected at those depths. The deep targets are the strongest features in the cross section, when corrected for the electric field strength. The results are consistent with the surface data, which also contain strong surface conversions along with deeper conversions.

Thompson et al. (2005) expand on the interpretation of these data, along with additional data. In Figure 17, the marked ES event near 1300 m ties very well with seismic data and the lateral extent of the ES data ties with known reservoir boundaries, including a fault that terminates the east side of the reservoir.

CONCLUSIONS

The binary-coded waveform is a particularly flexible tool for ES detection. The individual elements in the waveform determine the frequency content. They are adjustable for targets of varying depths. Design of the related binary sequence minimizes correlation side lobes and discriminates between linear and nonlinear conversion mechanisms. The long waveforms, with lengths of ~ 30 s, effectively detect small desired signals in a field containing much random noise and many unwanted conversions.

The PWS efficiently implements the binary-coded waveform and is an important component of the overall ES exploration system. The full system includes presurvey modeling, electrode design and implementation, pickup-free geophones, and acquisition and processing to minimize noise. When all the components are working effectively, the data acquisition system detects both linear and nonlinear ES conversions.

ACKNOWLEDGMENTS

We acknowledge the support of Exxon Mobil Production Department for assisting during the field tests. We acknowledge the work of Mesa Engineering for the design and construction of our PWS units. We also acknowledge the many colleagues at Exxon Mobil Upstream Research and Exxon Mobil Corporate Strategic Research who contributed so much to the theory, modeling, and field implementation of the ES method. We particularly acknowledge the management of Exxon Mobil Upstream Research Company for their support over many years of research.

APPENDIX A

DYNAMIC RANGE

The dynamic range of a recording system is the range of amplitudes that can be represented by the recorded bits after digitization. The largest expected signals fix the top of this range. Situations can arise wherein small signals fall beneath the resulting range. In ES recording, the converted seismic signal is often quite small and falls below the least significant bit (LSB). The recorded random noise, on the other hand, will generally be much larger than the LSB.

This appendix is included because the ES detection system is claimed to be sensitive to particle velocities less than 10^{-13} m/s. In calculations designed to estimate the ultimate practical sensitivity of the ES system, we find that it may even be necessary to detect signals several orders of magnitude smaller than reported here. Detection of such small signals naturally raises questions about the physical limits on sensitivity. Here we show that the digitization process does not necessarily limit the sensitivity.

Consider the situation in which the random noise is much larger than the amplitude of the LSB in a recording system. A small signal, sinusoidal for example, is then added to this noise prior to recording. The amplitude of the added sinusoid is less than the LSB. The signal plus noise is quantized and digitized for recording.

An example of this is illustrated in Figure A-1. A low level sinusoidal signal (shown) of peak amplitude 3×10^{-4} is added to standard normal Gaussian noise (not shown). The resulting sum is then quantized to the nearest 1/128 and compared with the quantized result of the noise alone. (This level of quantization is quite coarse and is meant only for illustration.) Altered samples [$Q(\text{sig} + \text{nse}) - Q(\text{nse})$] represent the samples where the LSB has been affected by

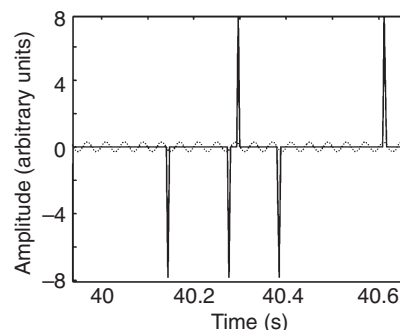


Figure A-1. Altered samples, the sharp spikes, after adding a low-level sine wave to standard normal Gaussian noise (not shown) followed by quantization at 1/128. The altered samples are the function $[Q(\text{sig} + \text{nse}) - Q(\text{nse})]$.

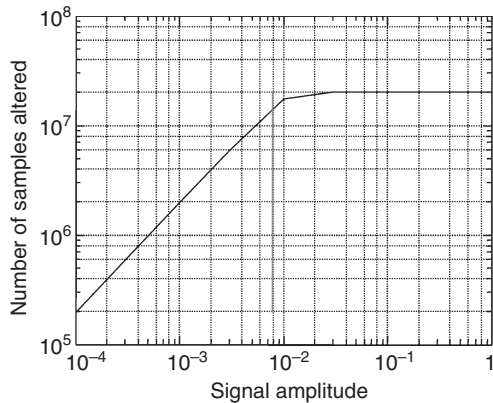


Figure A-2. Number of altered samples from quantization of noise when signal is added as a function of signal strength. Below the quantization step size of 8×10^{-3} , the number of samples increases linearly with the signal amplitude.

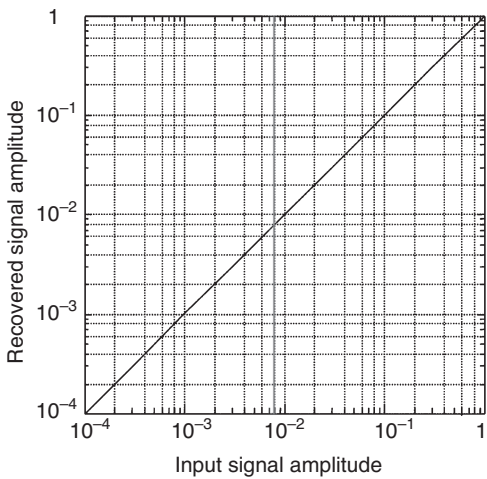


Figure A-3. The amplitude of the correlation peak after correlation with the altered samples from quantization, i.e., with $Q(\text{sig} + \text{nse}) - Q(\text{nse})$. The reference is scaled such that a sinusoidal signal of unit amplitude will give a correlated value of one. A single 100-s trace with 4-ms sample interval is correlated.

the presence of the sinusoidal signal. This difference appears as the set of spikes.

Note that the altered samples always have the same sign as the underlying signal. As a result, correlation of the altered samples with a sinusoidal reference will give a positive peak. The number of altered samples also increases with the underlying signal amplitude. One would expect the correlation peak to be linear with the signal amplitude and this, in fact, turns out to be the case.

Figure A-2 is a plot of the number of altered samples versus the added sinusoidal signal amplitude. A noise record with 2×10^7 standard normal noise samples is quantized with quantization step size of 1/128. This is compared with the quantized result when a sinusoid of varying amplitude is added prior to quantization.

The number of altered samples varies linearly with the sinusoidal amplitude (log-log slope of one) for signal amplitudes less than the quantization step size. As the sinusoidal peak amplitude passes the quantization step size, the added signal affects nearly all the samples.

Figure A-3 illustrates the final issue of correlation amplitude. In this example, the altered samples from quantization [i.e., $Q(\text{sig} + \text{nse}) - Q(\text{nse})$] are correlated with a sinusoidal reference. The reference is scaled such that a sinusoidal signal of unit amplitude will give a correlated value of one. The peak values after correlation are plotted against the input signal amplitudes. For this example, a single 100-s trace with 4-ms sample interval is used. The amplitude after correlation matches the input amplitude over a wide range of signal amplitudes both smaller and larger than the quantization step size.

These comments about recovered amplitudes deal with the expected amplitudes when there are a large number of samples; that is, long correlated sweeps and/or many repetitions. For extremely small signal amplitudes, only a small number of quantized samples are affected by the signal. This can lead to some undesirable quantization effects. In this case, the recovered amplitude is inaccurate and correlation side lobes from the small signal are large.

REFERENCES

- Ashcroft, N. W., and N. D. Mermin, 1976, Solid state physics: Holt, Rinehart, and Winston, 590.
- Claerbout, J. F., 1985, Imaging the earth's interior: Blackwell Scientific Publications, Inc.
- Corson, D. R., and P. Lorrain, 1962, Introduction to electromagnetic fields and waves: Freeman and Co.
- Foster, M. R., and R. W. Sloan, 1972, The use of pseudonoise sequences to code a pulsed neutron logging source: Geophysics, **37**, 481–487.
- Golay, M. J. E., 1961, Complementary series: IRE Transactions on Information Theory, **7**, 82–87.
- Golomb, S., 1964, Digital communications with space applications: Prentice-Hall Inc.
- Hornbostel, S. C., and A. H. Thompson, 2002, Source waveforms for electroseismic exploration: U. S. Patent 6,477,113 B2.
- Hornbostel, S. C., A. H. Thompson, T. C. Halsey, R. A. Raschke, and C. A. Davis, 2003, Nonlinear electroseismic exploration: U. S. Patent 6,664,788 B2.
- Kounias, S., C. Koukouvinos, and K. Sotirakoglou, 1991, On Golay sequences: Discrete Mathematics, **92**, 177–185.
- Pride, S., 1994, Governing equations for the coupled electromagnetics and acoustics of porous media: Physical Review B, **50**, 15678–15696.
- Thompson, A. H., S. C. Hornbostel, J. S. Burns, T. J. Murray, R. A. Raschke, J. C. Wride, P. Z. McCammon, J. R. Sumner, G. H. Haake, M. S. Bixby, W. S. Ross, B. S. White, M. Zhou, and P. K. Peczak, 2005, Field tests of electroseismic hydrocarbon detection: 75th Annual International Meeting, SEG, Expanded Abstracts, 565–568.
- White, B. S., 2005, Asymptotic theory of electroseismic prospecting: SIAM Journal on Applied Mathematics, **65**, 1443–1462.
- Widrow, B., and J. R. Glover Jr., 1975, Adaptive noise canceling: Principles and applications: Proceedings of the Institute of Electrical and Electronics Engineers, **63**, 1692–1716.